

# A variable DNA recognition site organization establishes the LiaR-mediated cell envelope stress response of enterococci to daptomycin

Milya Davlieva<sup>1</sup>, Yiwen Shi<sup>1</sup>, Paul G. Leonard<sup>2,3</sup>, Troy A. Johnson<sup>2,3</sup>, Michael R. Zianni<sup>4</sup>, Cesar A. Arias<sup>5,6,7</sup>, John E. Ladbury<sup>3,8</sup> and Yousif Shamoo<sup>1,\*</sup>

<sup>1</sup>Department of BioSciences, Rice University, Houston, TX 77005, USA, <sup>2</sup>Department of Genomic Medicine, The University of Texas MD Anderson Cancer Center, Houston, TX 77030, USA, <sup>3</sup>Center for Biomolecular Structure and Function, The University of Texas MD Anderson Cancer Center, Houston, TX 77030, USA, <sup>4</sup>Plant-Microbe Genomics Facility, The Ohio State University, Columbus, OH 43210, USA, <sup>5</sup>Division of Infectious Diseases, Department of Internal Medicine, University of Texas Medical School at Houston, Houston, TX 77030, USA, <sup>6</sup>Department of Microbiology and Molecular Genetics, The University of Texas Health Science Center at Houston, Houston, TX 77030, USA, <sup>7</sup>Molecular Genetics and Antimicrobial Resistance Unit, Universidad El Bosque, Bogota, 110121, Colombia and <sup>8</sup>Department of Biochemistry and Molecular Biology, The University of Texas MD Anderson Cancer Center, Houston, TX 77030, USA

Received November 26, 2014; Revised March 27, 2015; Accepted March 30, 2015

## ABSTRACT

**LiaR is a ‘master regulator’ of the cell envelope stress response in enterococci and many other Gram-positive organisms. Mutations to *liaR* can lead to antibiotic resistance to a variety of antibiotics including the cyclic lipopeptide daptomycin. LiaR is phosphorylated in response to membrane stress to regulate downstream target operons. Using DNA footprinting of the regions upstream of the *liaXYZ* and *liaFSR* operons we show that LiaR binds an extended stretch of DNA that extends beyond the proposed canonical consensus sequence suggesting a more complex level of regulatory control of target operons. We go on to determine the biochemical and structural basis for increased resistance to daptomycin by the adaptive mutation to LiaR (D191N) first identified from the pathogen *Enterococcus faecalis* S613. LiaR<sup>D191N</sup> increases oligomerization of LiaR to form a constitutively activated tetramer that has high affinity for DNA even in the absence of phosphorylation leading to increased resistance. Crystal structures of the LiaR DNA binding domain complexed to the putative consensus sequence as well as an adjoining secondary sequence show that upon binding, LiaR induces DNA bending that is consistent with increased recruitment of RNA polymerase to the transcription start site and upregulation of target operons.**

## INTRODUCTION

Vancomycin-resistant enterococci are important contributors to the rise of multi-drug resistant Hospital-Associated Infections (HAIs) and in 2013 were categorized as a ‘serious’ threat by the Centers for Disease Control and Prevention (CDC). HAIs are common complications of hospitalization and it is postulated that these infections cause over 2 million cases, and at least 23 000 deaths per year in the United States (<http://www.cdc.gov/drugresistance/threat-report-2013/>). Perhaps, surprisingly, the majority of HAIs are caused by a handful of organisms. The organisms most strongly associated with US hospital infections and to which new antibiotics are urgently needed are frequently referred to as the no ‘ESKAPE’ pathogens (*Enterococcus faecium*, *Staphylococcus aureus*, *Klebsiella pneumoniae*, *Acinetobacter baumannii*, *Pseudomonas aeruginosa*, *Enterobacter* spp.) (1,2). Among the no ‘ESKAPE’ organisms, vancomycin-resistant enterococci (VRE) are of particular concern due to lack of reliable bactericidal therapeutic options. Enterococci (both *E. faecalis* and *E. faecium*) have become increasingly problematic in hospitals around the world with more than 80% of hospital-associated *E. faecium* isolates resistant to ampicillin and vancomycin (3). As a consequence, VRE present a substantial clinical threat and FDA-approved therapies, such as quinupristin/dalfopristin and linezolid, have important limitations due to resistance, toxicities and bacteriostatic effects against the most recalcitrant organisms. In response to the increased frequency of clinical resistance, the lipopeptide daptomycin is often used ‘off-label’ as an antibiotic of last resort for enterococci (3).

\*To whom correspondence should be addressed. Tel: +1 713 348 5493; Fax: +1 713 348 4105; Email: shamoo@rice.edu

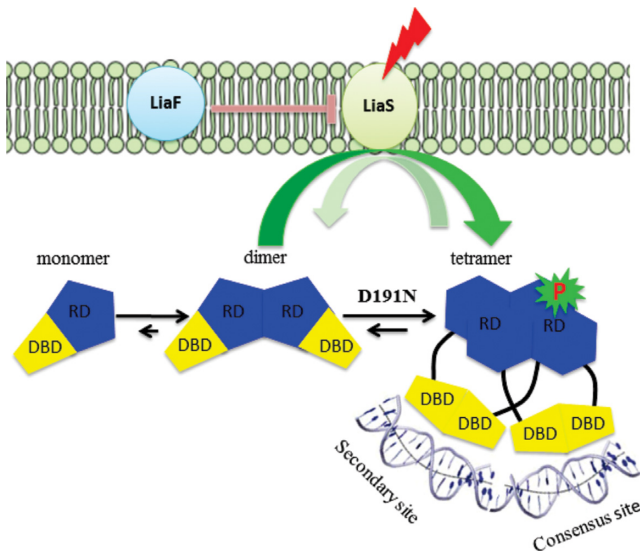


**Figure 1.** LiaFSR signaling pathway. In the absence of cell membrane-acting antibiotics, the three-component regulatory system, LiaFSR, is turned ‘OFF’ by the negative interaction of LiaF with LiaS. LiaS responds to membrane stress by phosphorylation of LiaR leading to downstream changes in the transcription of several operons to affect membrane homeostasis. *E. faecalis* LiaR is present largely as a dimer at physiologically relevant concentrations. Phosphorylation, or mutation to a constitutively active analog like LiaR<sup>D191N</sup>, induces changes in the conformation of the receiver domain leading to release of DNA binding domain and promoting a self-dimerization event to form an active tetramer able to bind extended DNA sequences. Abbreviations: RD, receiver domain; DBD, DNA binding domain.

Using clinical-strain pairs of DAP-resistant and susceptible *E. faecalis* recovered from a patient before and after therapy, we showed that mutations in *liaFSR*, encoding a three-component regulatory system, were responsible for the resistance phenotype (4). Using quantitative experimental evolution, we subsequently demonstrated that the most common evolutionary trajectories leading to daptomycin resistance were indeed through changes in the LiaFSR pathway (5). The LiaFSR system is composed of LiaS, a membrane-bound protein histidine kinase; LiaR, a cytosolic response regulator and LiaF, a membrane-bound protein that reduces or attenuates LiaS activity (Figure 1) (6–9).

Mutations to LiaF, LiaR and LiaS have already been identified associated with DAP-resistance in clinical isolates of enterococci and are the most common adaptive changes in response to daptomycin (4,5,10–12). Moreover, we recently showed that deletion of *liaR* in a DAP-resistant strain of *E. faecalis* reversed the DAP resistance phenotype and markedly increased susceptibility to other cell-membrane acting antibiotics and antimicrobial peptides with different mechanism of action. Most importantly, the lack of *liaR* was associated with hypersusceptibility to DAP in a laboratory strain of *E. faecalis*, supporting the idea of LiaR as a ‘master regulator’ of the enterococcal cell membrane stress response (13).

Using *in silico* analysis, we identified a potential *liaR* binding site upstream from a gene cluster encoding three proteins of unknown function (designated *liaXYZ*, for-

merly *ylbB*, *pspC*, *ylvD*). Moreover, we previously showed that an adaptive mutation in LiaX (*liaX*<sup>I-289</sup>) (5) confers increased resistance to daptomycin, suggesting that this cluster is regulated by LiaR. Thus, the identification of potential LiaR regulatory sequences upstream of the *liaFSR* and *liaXYZ* operons along with our earlier observation that mutation of *liaX* was sufficient to increase resistance to daptomycin formed the basis for the inclusion of the *liaXYZ* operon in this study. Based on earlier studies of *B. subtilis* *liaRS*, we reasoned that adaptive changes to LiaR would likely activate the *liaFSR* regulon more strongly or even produce a constitutive ‘on’ response that remodels the membrane to reduce antibiotic susceptibility (6).

To elucidate the physicochemical basis for *E. faecalis* LiaR-mediated changes in daptomycin susceptibility, we used a combination of biophysical and structural approaches to map and quantitate the binding of LiaR and several LiaR variants to the upstream regulatory sequences of both the *liaFSR* and *liaXYZ* operons. Our studies reveal that activation of LiaR hinges on a dimer to tetramer transition (Figure 1) that allows LiaR to recognize complex upstream regulatory regions that extend beyond the predicted consensus sequence. Strikingly, the adaptive mutation LiaR<sup>D191N</sup> shifts LiaR into the activated tetramer even in the absence of phosphorylation leading to a constitutively ‘on’ state. Crystal structures of the LiaR DNA binding domain bound to both the consensus sequence and an adjoining secondary site suggest that LiaR binding significantly bends DNA as part of its potential recruitment of RNA polymerase. As a ‘master’ regulator of the cell envelope stress response, LiaR, as well as other components of the LiaFSR system, may prove to be excellent targets for the development of new strategies and drugs that alter membrane adaptation and, perhaps, would prevent the evolution of resistance in enterococci or other organisms thereby extending the efficacy of current drugs. It is also clear that an increasing number of well-studied transcriptional regulators such as ArcA, BvgA, ComA and UhpA (14–17) may also bind to more complex and nuanced DNA regulatory structures. Presumably such sophisticated regulation reflects robust tuning through evolutionary selection of regulators and their accompanying networks to allow rapid adaptation to changing environments (18).

## MATERIALS AND METHODS

### Expression and purification of *E. faecalis* LiaR and its variants

The LiaR gene and truncated LiaR gene (residues 140–206 of LiaR from *E. faecalis* S613, LiaR<sup>(DBD)</sup>) were amplified by PCR from genomic DNA S613 and cloned into pETDuet vector. Site-directed mutagenesis of LiaR was performed using the Stratagene QuikChange™ Site-Directed Mutagenesis Kit (Stratagene, La Jolla, CA, USA). Recombinant proteins were expressed in *Escherichia coli* BL21 (DE3) at 30°C in EnPresso™ or EnPresso B culture medium (Biosilta, Oulu, Finland) and purified with a HisTrap affinity column (GE Healthcare) followed by the anion-exchange chromatography and gel filtration for the final step (Supplemental Information).

### DNA footprint analysis by automated capillary electrophoresis (DFACE)

The DFACE procedure was performed as described previously (Supplemental Information) (19,20).

### Determination of DNA binding affinity by Microscale Thermophoresis

The affinity of LiaR and LiaR variants for duplex DNAs were measured by MicroScale Thermophoresis (MST) (21). MST experiments were performed on a Monolith NT.115 system (Nanotemper Technologies) using 25% LED and 100% IR-laser power. Measurements were also carried out on 25% LED power and 90% IR-Laser power for comparison. The resulting  $K_d$  values based on average from six independent MST measurements. Data analyses were performed using Nanotemper Analysis software, v.1.5.41.

### Analytical ultracentrifugation

Sedimentation equilibrium analytical ultracentrifugation (SEQ) experiments were performed at 20°C using a Beckman XL-I instrument with an AnTi60 rotor. Data analysis was performed using Sedphat 10.40 (22,23). For each protein, the SEQ profiles were globally fitted to a either a dimer-tetramer (LiaR, LiaR<sup>D50E</sup> and LiaR<sup>D191N</sup>) or a monomer-dimer (LiaR<sup>(DBD)</sup>, LiaR<sup>(DBD)D191N</sup>) equilibrium model.

### Structure determination of LiaR<sup>(DBD)</sup> and LiaR<sup>(DBD)D191N</sup>

Crystals of DBD LiaR suitable for data collection were obtained in 0.1 M Tris pH 8.6, 0.2 M LiSO<sub>4</sub>, 20% (w/v) PEG 3.350, 0.05% Tween-20, 10% glycerol, 10 mM praseodymium (III) acetate hydrate. The diffraction data sets were collected at Argonne National Laboratory's Advanced Photon Source (ANL APS) beamline 21-ID-F on a MarMosaic 225 CCD detector. The structure of LiaR<sup>(DBD)</sup> protein was solved by molecular replacement (24) using the DNA binding domains of berylliofluoride-activated VraR from *Staphylococcus aureus* (PDB code: 4IF4) as an initial search model. The solution from molecular replacement suggested two molecules in the asymmetric unit and a Matthews coefficient of 3.03 (59.5% solvent content) (25). The initial model was submitted to phenix.autobuild and phenix.refine for automatic building and structure refinement (26). Phenix.Xtriage (26) analysis was performed for initial data characterization. Data analysis suggested that pseudo-merohedral twinning by the twin law,  $-h, l, k$ , was possible; however, no significant pseudotranslation was detected by Patterson analysis. Structural refinement was carried out in Phenix: phenix.refine (26) with the twin specific target function. The initial model was improved by iterative rebuilding using  $(2F_o - F_c)$  a map made with Coot (27). The applicable pseudo-merohedral twin law,  $-h, l, k$ , was applied from the beginning and throughout refinement in Phenix.refine and the twin fraction reached a final value of 0.49. Water molecules were added using phenix.refine program and by manual inspection of  $2F_o - F_c$  electron density maps. The structure of the LiaR<sup>(DBD)D191N</sup> protein was solved by molecular replacement (24) using the LiaR<sup>(DBD)</sup>

structure as an initial search model. Structural refinement was carried out in Phenix: phenix.refine with the twin specific target function ( $-h, l, k$ , twin fraction is 0.49) (Supplemental Information). Ramachandran plots and root mean square deviations from ideality for bond angles and lengths for LiaR<sup>(DBD)</sup> and LiaR<sup>(DBD)D191N</sup> were determined using the structure validation program MolProbity (28). Structure factors and final atomic coordinates have been deposited with the Protein Data Bank (entries: 4WSZ and 4WT0, respectively)

### Structure determination of LiaR<sup>(DBD)D191N</sup> with DNA

The crystal used in the DBD LiaR<sup>D191N</sup>/26-bp DNA structure was crystallized with 0.08 M KCl, 0.02 M BaCl<sub>2</sub>, 0.04 M sodium cacodylate (pH 6.0), 43% MPD, 0.012 M spermine tetrachloride, 0.01 M proline, 0.01 M strontium chloride. Crystals of the DBD LiaR<sup>D191N</sup>-22 bp DNA complex were grown in 0.03 M Bis-Tris propane/3.4, 0.07 M citric acid, 18% PEG 3350, 0.05% N,N-dimethyldodecylamine N-oxide, 0.1 M sodium malonate. The single wavelength (0.9788 Å) data sets were collected at (ANL APS) beamline 21-ID-D on a MarMosaic 300 CCD detector. Molecular replacement method was used to determine the structures of DNA-protein complexes using the DBD LiaR<sup>D191N</sup> (PDB 4WT0) as a search model (Supplemental Information) (PDB: 4WUL and 4WU4).

## RESULTS AND DISCUSSION

### DNA footprinting analysis of the upstream regions of *liaXYZ* and *liaFSR* reveal a larger than expected LiaR recognition sequence

A comparison of the DNA sequences upstream of the *liaXYZ* and *liaFSR* operons and comparable operons from *Bacillus subtilis* and *S. aureus* (7,29) suggested that LiaR recognizes a T(X)<sub>4</sub>C(X)<sub>4</sub>G(X)<sub>4</sub>A consensus motif (5). The degeneracy of potential sequences upstream of other putative LiaR target operons also suggested that LiaR-mediated regulation might be substantially more nuanced than a simple single consensus sequence (30). DNase I Footprinting followed by Automated Capillary Electrophoresis (DFACE) was used to delineate the LiaR footprint and identify potential target sequences for further physicochemical analysis (Figure 2). Our initial binding studies suggested that unphosphorylated LiaR had no measurable affinity for either operon but that the adaptive mutant LiaR<sup>D191N</sup> had substantially increased affinity for the *liaXYZ* operon. We therefore used LiaR<sup>D191N</sup> as a proxy for activated LiaR in our footprinting experiments. DFACE analysis of the *liaXYZ* promoter region from -320 to +30 provided clear evidence for a contiguous protected region approximately 43 bp in length that extended from position -120 to -77. LiaR<sup>D191N</sup> binds to an extended region of the DNA that includes not only the predicted consensus region (-99 to -84) (5), but also the DNA sequences from -100 to -120. We refer to these protected regions outside the consensus sequence as 'secondary sequences.' In addition to the protected sequences, we observed a distinct DNase I hypersensitive site at position -83 next to the adenine (underlined) of the T(X)<sub>4</sub>C(X)<sub>4</sub>G(X)<sub>4</sub>A consensus sequence



(Figure 2A). To assess the concentration-dependence of the LiaR footprint, DFACE experiments were performed at 0.5 and 5.0  $\mu\text{M}$  LiaR. Overall, the amount of protection at each position increased modestly at 5.0  $\mu\text{M}$  protein but the pattern did not vary significantly with the notable exceptions of A(−84) and the hypersensitive site T(−83) where protection and reactivity increased, respectively. Protein concentration-dependent DNaseI hypersensitivity at T(−83) suggests that LiaR binding may alter the structure or curvature of the DNA allowing more efficient DNaseI cleavage. Based on sequence homology to other response regulators, the active species of LiaR would be expected to dimerize and have a site size of  $\sim 21$  nucleotides. Our protection experiments identified a region of protection that was twice the size expected for the simple binding of an activated LiaR dimer to DNA.

Previous studies on LiaR homologs had suggested that LiaR also regulates its own operon and inspection of the 5' region of the *liaFSR* operon revealed two potential consensus sites. We used DFACE to establish the LiaR binding footprint and to observe whether LiaR binding to the *liaFSR* operon would produce an extended binding site comparable to that observed for the *liaXYZ* operon. We mapped LiaR binding over the region from −367 to +30 and observed that only the region from −97 to −68 had significant and contiguous protection when incubated with 0.5  $\mu\text{M}$  LiaR<sup>D191N</sup> (Figure 2C). The potential second consensus binding site at position −258 to −243 did not show any protection (data not shown). There were no significant changes in the size of the footprint or degree of protection in the presence of 5  $\mu\text{M}$  protein compared to 0.5  $\mu\text{M}$ . As with the *liaXYZ* operon, we observed a strong hypersensitive site at T(−78) the nucleotide following the adenine (underlined) of T(X)<sub>4</sub>C(X)<sub>4</sub>G(X)<sub>4</sub>A consensus sequence (Figure 2C). It is interesting that the *liaFSR* hypersensitive site is located at the same relative position, e.g. one nucleotide 3' of the consensus sequence suggesting that protein binding imposes a similar change in DNA backbone structure and accessibility of both the *liaXYZ* and *liaFSR* regulatory regions. The LiaR footprint on the *liaFSR* operon has an additional hypersensitive site at C(−89) that is not present in the LiaR:*liaXYZ* footprint (Figure 2C). Overall, the most striking difference in the protection patterns for the two operons is the length of the protected regions. The size of the protection site for *liaFSR* is about 29 bases while that of *liaXYZ* was 43 bases. Interestingly, LiaR protection for the *liaFSR* operon extends about 10 bases toward the downstream translation start site, while the *liaXYZ* protection pattern extends away from the consensus sequence in the upstream direction. A different orientation for the extended protection regions suggests that recognition sequences outside the consensus motif can be oriented in either direction and is consistent with a versatile regulatory architecture.

#### Phosphomimetic mutant LiaR<sup>D50E</sup> increases affinity for DNA

Phosphorylation of LiaR leads to activation of target operons to mitigate cell envelope stress (6). Based on a comparison of the *E. faecalis* LiaR sequence with that of other response regulators from NarL/FixJ subfamily (*S. aureus*

VraR, *B. subtilis* LiaR, *E. coli* NarL, FixJ) we identified Asp-50 as a potential site for phosphorylation (31). We were unable to find *in vitro* conditions that led to quantitative and stable phosphorylation of *E. faecalis* LiaR using small-molecule phosphoryl donors, such as acetyl phosphate or phosphoryl-mimics such as beryllium fluoride (32). Therefore, in order to perform biochemical studies on the phosphorylated LiaR, we mutated the putative phosphorylation site Asp-50 to a glutamate to produce a potentially stable and constitutively active mutant.

We tested the affinity of LiaR and LiaR<sup>D50E</sup> for the region encompassing the consensus sequences by Microscale Thermophoresis (MST) (Figure 3). Since our DNA footprinting had clearly identified an extended region of protection that included the putative consensus sequences for the *liaXYZ* operon, we tested the affinity of LiaR for both the consensus and adjoining secondary sites separately as well as together to make an extended sequence that included the entire DNA footprint region (Figure 2B). Although wild type LiaR affinity for DNA was too low to estimate an accurate  $K_d$ , the putative phosphomimetic mutant, LiaR<sup>D50E</sup>, had substantially increased affinity (Table 1, Figure 3A). Our observed  $K_d$  of  $4.13 \pm 0.48 \mu\text{M}$  for the *liaXYZ* consensus sequence is consistent with the *in vivo* measurements made for the *S. aureus* homolog of LiaR, VraR suggesting regulation of relevant operons in the micromolar range (29,33). Given that the mutation of Asp-50 to glutamate is not identical to phosphorylation of aspartate, it may well be that the additional electronegative character of phosphoaspartate may further increase the  $K_d$  for specific DNA sequences. As expected, mutation of the putative phosphorylation site to alanine (LiaR<sup>D50A</sup>) decreased LiaR affinity for either sequence below detectable levels. These data are consistent with Asp-50 as the site of phosphorylation and the low affinity of unphosphorylated LiaR for target DNA.

#### Adaptive mutant LiaR<sup>D191N</sup> that confers increased daptomycin resistance in *E. faecalis* S613 dramatically increases LiaR affinity for target DNA sequences

In a previous study, we had recovered the mutant LiaR<sup>D191N</sup> that confers increased daptomycin resistance (5). In contrast to the weak, nearly non-detectable affinity of LiaR for the individual *liaXYZ* and *liaFSR* sites, the adaptive mutant LiaR<sup>D191N</sup> had dramatically increased affinity for all the DNA sequences we measured (Table 1, Figure 3). LiaR<sup>D191N</sup> had at least a 100-fold increase in the DNA binding affinity to either the *liaXYZ* or *liaFSR* consensus sequences compared to wild type LiaR and exhibited 10–500-fold higher affinity to the target sequences than the phosphomimetic mutant LiaR<sup>D50E</sup>. Binding to the *liaXYZ* secondary site was also strongly increased suggesting an overall increase in affinity for DNA. Surprisingly however, LiaR<sup>D191N</sup> affinity for the entire contiguous protected region identified by DNA footprinting for *liaXYZ* (46 nucleotides, see Figure 2B) was comparable to that for the consensus site alone (*liaXYZ*:  $K_d = 0.63 \pm 0.04 \mu\text{M}$  versus  $0.39 \pm 0.03 \mu\text{M}$  (Table 1)). These results reveal that despite being protected in our nuclease protection assays, the additional secondary region protected within the *liaXYZ* operon is not required for high affinity binding. Remark-

**Table 1.** DNA binding affinity of *E. faecalis* S613 LiaR and variants

Protein	<i>liaXYZ</i> consensus $K_d$ [ $\mu$ M]	<i>liaXYZ</i> secondary $K_d$ [ $\mu$ M]	<i>liaFSR</i> consensus $K_d$ [ $\mu$ M]	<i>liaFSR</i> extended $K_d$ [ $\mu$ M]	<i>liaXYZ</i> entire protected $K_d$ [ $\mu$ M]	<i>liaFSR</i> entire protected $K_d$ [ $\mu$ M]
LiaR	N/D <sup>a</sup>	N/D <sup>a</sup>	N/D <sup>a</sup>	N/D <sup>a</sup>		
LiaR <sup>D50E</sup>	4.13 $\pm$ 0.48	Weak <sup>b</sup>	Weak <sup>b</sup>	>250		
LiaR <sup>D191N</sup>	0.39 $\pm$ 0.03	21.9 $\pm$ 4.5	>150	0.37 $\pm$ 0.02	0.63 $\pm$ 0.04	0.88 $\pm$ 0.04
LiaR <sup>D50A</sup>	N/D <sup>a</sup>	N/D <sup>a</sup>	N/D <sup>a</sup>	>250		
LiaR <sup>D50E/D191N</sup>	3.63 $\pm$ 0.55	16.1 $\pm$ 2.10	N/D <sup>a</sup>	2.8 $\pm$ 0.30		
LiaR <sup>DBD</sup>	N/D <sup>a</sup>	N/D <sup>a</sup>	N/D <sup>a</sup>	N/D <sup>a</sup>		
LiaR <sup>(DBD)D191N</sup>	4.06 $\pm$ 0.76	Weak <sup>b</sup>	>150	1.88 $\pm$ 0.08		

<sup>a</sup>No detectable binding by MST up to 466  $\mu$ M LiaR, 224  $\mu$ M LiaR<sup>D50A</sup>, 344  $\mu$ M LiaR<sup>DBD</sup>, 138  $\mu$ M LiaR<sup>D50E/D191N</sup>.

<sup>b</sup>At the concentration range of this experiment setup, a small change in thermophoresis was observed, but it was not large enough to confidentially report a binding value.

ably, the increased affinity of LiaR<sup>D191N</sup> for target DNA exceeded that of the phosphomimetic mutant LiaR<sup>D50E</sup> suggesting that the adaptive mutant is activated irrespective of its potential phosphorylation state. To test whether the mutations LiaR<sup>D50E</sup> and LiaR<sup>D191N</sup> functioned cooperatively or independently of each other, we made the double mutant LiaR<sup>D50E/D191N</sup> and measured its affinity for the *liaXYZ* and *liaFSR* sequences. The double mutant had affinity most like the single mutant LiaR<sup>D50E</sup> suggesting negative epistasis between the alleles. Our data is consistent with a model in which LiaR<sup>D191N</sup> is a constitutively activated or, perhaps, even a hyperactivated protein.

#### *liaFSR* consensus sequence is not sufficient for tight binding by LiaR

We tested the affinity of LiaR<sup>D191N</sup> for a 26 nucleotide DNA that contained only the putative *liaFSR* consensus sequence extending from  $-104$  to  $-79$ . Surprisingly, wild type LiaR, adaptive mutant LiaR<sup>D191N</sup>, and phosphomimetic mutant LiaR<sup>D50E</sup> all had very low affinity for the sequence that was comparable in length and sequence to the high affinity site we had identified in the *liaXYZ* operon. The affinity of LiaR<sup>D191N</sup> for the *liaFSR* consensus was at least 400-fold lower than the *liaXYZ* consensus sequence (Table 1). DFACE had suggested that the footprint of LiaR on the *liaFSR* operon extended from the consensus sequence  $\sim 10$  bases toward the translation start site. Based upon this DNA protection data, we extended the DNA sequence an additional six nucleotides to include the entire protected region. LiaR<sup>D191N</sup> affinity for the extended 31 nucleotide sequence increased dramatically to  $0.37 \pm 0.02 \mu$ M making it nearly identical to the high affinity we observed for the *liaXYZ* consensus sequence ( $0.39 \pm 0.03 \mu$ M) (See Figure 2B, D, Figure 3B and Table 1). When we scrambled the extended downstream site of *liaFSR* (11 nucleotides: ATGTACGAGCT) the LiaR<sup>D191N</sup> binding affinity decreased  $\sim 3$ -fold ( $K_d = 1.35 \pm 0.08 \mu$ M) but was still higher than for the consensus site alone ( $K_d > 150 \mu$ M) suggesting that both sequence and length of this additional protected region are critical for the binding affinity. Our findings suggest that the additional region protected within the *liaFSR* binding site (six nucleotides: ACCTGA) is likely important for LiaR binding and positioning relative to the transcriptional start site.

Importantly, our data suggests that the T(X)<sub>4</sub>C(X)<sub>4</sub>G(X)<sub>4</sub>A *liaFSR* consensus sequence, unlike that of *liaXYZ*, is not sufficient for high affinity binding and that other nucleotides within and proximal to the consensus sequence can have an important role in attenuating LiaR affinity for target DNA. That these extended DNA sequences have comparable affinities but different ways of realizing increased affinity suggests that each regulatory region is unique and contextualized to the specific operon.

#### Oligomerization of LiaR to tetramers suggests a potential mechanism for extended DNA target recognition

Studies of the related response regulator *S. aureus* VraR and the more widely characterized OmpR/PhoB winged-helix transcription factor response regulator subfamily have suggested that a phosphorylation-dependent oligomerization from monomer to dimer is frequently responsible for recognition of specific DNA target sequences (31,32,34). We were therefore surprised that analytical ultracentrifugation analysis (AUC) indicated that the best fit for data obtained on the full length LiaR was a dimer-tetramer equilibrium model with a  $K_d$  of 24  $\mu$ M (Figure 4A, B). Mutation of the Asp-50 phosphorylation site to glutamic acid further increased the extent of tetramerization ( $K_d = 2 \mu$ M) suggesting that oligomer formation would be stimulated by phosphorylation. The correlation of tetramer formation to functional consequences for LiaR recognition of DNA is further reinforced by our observation that the adaptive mutant LiaR<sup>D191N</sup> is nearly entirely tetrameric. The extent of LiaR<sup>D191N</sup> tetramerization is so strong that we were unable to observe free dimer and could only estimate the  $K_d$  to be  $< 0.06 \mu$ M—at least a 400-fold increase in tetramer formation compared to wild type LiaR. The best fits for all the LiaR variants were obtained with a model for dimer to tetramer equilibrium. Additionally, LiaR and its variants eluted during gel filtration as a broad peak with elution volumes, corresponding to the tetrameric and dimeric forms of LiaR, respectively with no evidence for either monomer or higher order oligomers (data not shown). The striking correlation of tetramer formation with increased DNA affinity from our MST studies suggests that *E. faecalis* LiaR does not follow the more canonical activation of a monomer to dimer species but rather is already present largely as a

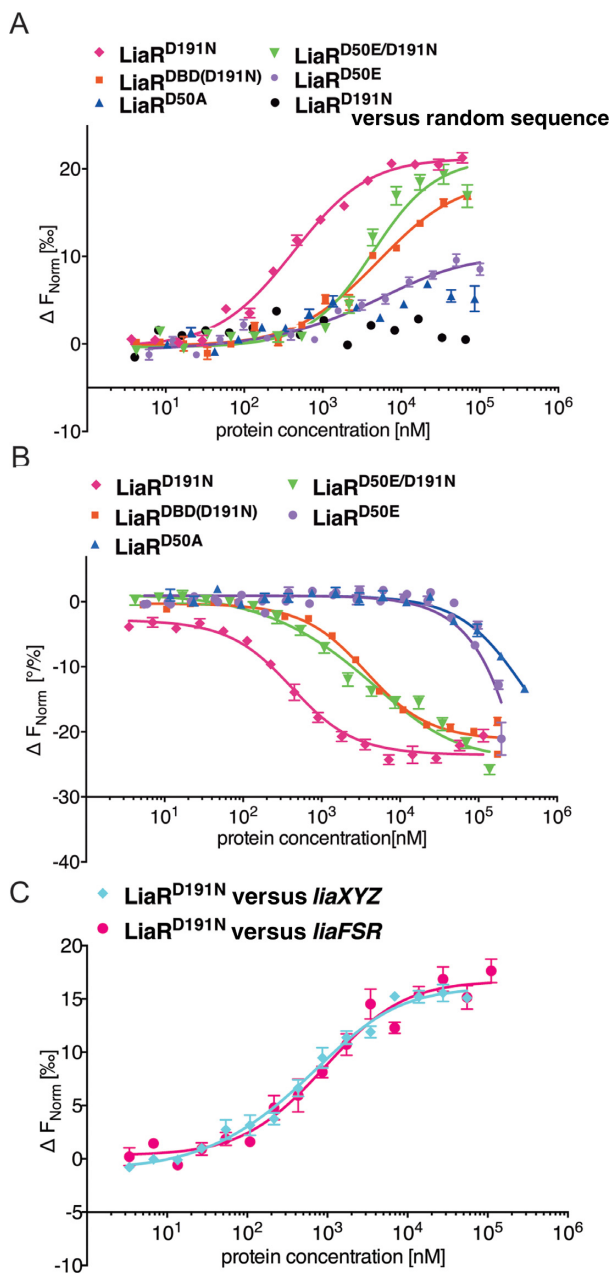


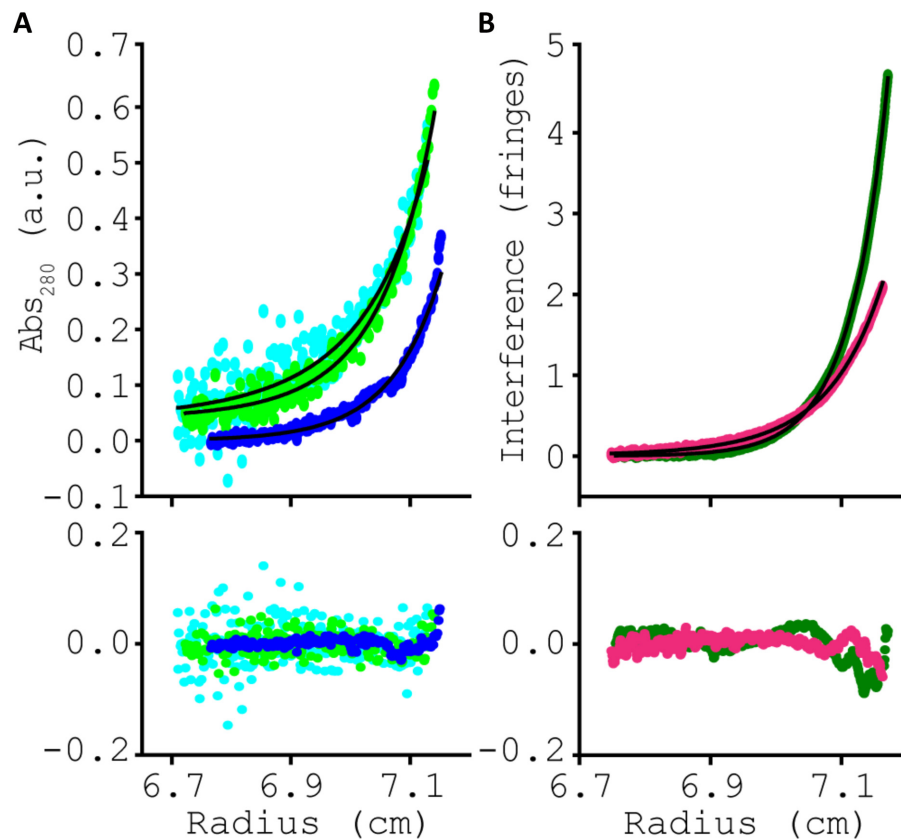
**Figure 3.** Adaptive mutant LiaR<sup>D191N</sup> that confers increased daptomycin resistance in *E. faecalis* S613 dramatically increases LiaR affinity for target DNA sequences. *E. faecalis* response regulator LiaR–DNA interactions were measured with MST. To determine the  $K_d$ , increasing concentrations of LiaR<sup>D191N</sup> was added to 40 nM of fluorescently labeled DNAs (Supplementary Information).  $F_{\text{norm}}$  (normalized fluorescence) was plotted on the y-axis in per mil [%] unit (meaning every 1000) against the total concentration of the titrated partner on a log<sub>10</sub> scale on the x-axis (21). The resulting  $K_d$  values based on average from six independent MST measurements. Note, when the markers were increased in size for readability the error bars became covered in some cases. (A) The binding of LiaR<sup>D191N</sup> (magenta diamonds), LiaR<sup>D50E</sup> (purple circles), LiaR<sup>D50A</sup> (blue triangles), LiaR<sup>D50E/D191N</sup> (green triangles) and LiaR<sup>DBD(D191N)</sup> (red squares) to the consensus sequence within the *liaXYZ* operon or LiaR<sup>D191N</sup> with a random sequence (black circles). (B) The binding of LiaR<sup>D191N</sup> (magenta diamonds), LiaR<sup>D50E</sup> (purple circles), LiaR<sup>D50A</sup> (blue triangles), LiaR<sup>DBD(D191N)</sup> (red squares), LiaR<sup>D50E/D191N</sup> (green triangles) to the extended site of the *liaFSR* operon. (C) The binding of LiaR<sup>D191N</sup> to the entire contiguous protected regions (Figure 2B, D) of *liaXYZ* (cyan diamonds) and *liaFSR* (magenta circles).

dimer at physiologically relevant concentrations and that upon phosphorylation, or mutation to a constitutively active analog like LiaR<sup>D191N</sup>, shifts the oligomeric state to an active tetramer able to bind extended DNA sequences. Concentration of LiaR *in vivo* has not been determined, but has been reported for the closest homolog of LiaR the *S. aureus* VraR (29). The concentration of response regulator VraR from *S. aureus* increased from 2.3 to 6  $\mu\text{M}$  in the presence of cell wall stress (29), which is in good agreement with the maximum increase *in vitro* transcription product observed at 6  $\mu\text{M}$  VraR-P (33). Note, that the concentration of VraR in the absence of stress is in agreement with those determined for other response regulators, such as OmpR (3500 molecules) (35) and CheY (6000 molecules) (36).

### Studies of the isolated LiaR DNA binding domain suggests that an increased affinity for DNA by the adaptive mutant LiaR<sup>D191N</sup> is correlated with increased oligomerization

To better understand the physicochemical basis for the daptomycin resistance conferred by mutation of position 191 to Asn, we measured the DNA binding affinity and oligomeric states of the isolated DNA binding domain (residues 140–206) of wild type LiaR, and the adaptive mutant LiaR<sup>D191N</sup>. Like the full length LiaR, the isolated DNA binding domain of LiaR (LiaR<sup>(DBD)</sup>) had undetectable levels of binding to *liaXYZ* and *liaFSR* sequences (Table 1) and, similar to the full length LiaR<sup>D191N</sup>, LiaR<sup>(DBD)D191N</sup> had strongly increased binding to *liaXYZ* ( $K_d = 4.06 \pm 0.76 \mu\text{M}$ ) and extended *liaFSR* consensus sequences ( $K_d = 1.88 \pm 0.08 \mu\text{M}$ ). Overall, LiaR<sup>(DBD)D191N</sup> binding to target DNA was  $\sim 10$ -fold weaker than full-length protein and is consistent with a role for the receiver domain in protein–protein interactions that would bring two copies of LiaR together as an initial dimer that can then further oligomerize into a tetramer. Since the mutation at Asn-191 appears to constitutively activate LiaR in the absence of phosphorylation, the normal role of phosphorylation in stimulating oligomerization via the receiver domain may be effectively overruled by the D191N mutation.

We reasoned that since the adaptive mutation D191N is located in the C-terminal DNA binding domain and that oligomerization was well correlated to DNA recognition, that we could test the role of the adaptive mutation in driving the oligomeric state of LiaR by investigating the oligomerization properties of the isolated LiaR DNA binding domain. Using analytical ultracentrifugation, we observed that the wild type LiaR<sup>(DBD)</sup> has a modest monomer–dimer transition ( $K_d = 2 \mu\text{M}$ ). So, despite not having a receiver domain for activation by phosphorylation or mediation of protein–protein contacts, the DNA binding domain of LiaR alone can establish a dimeric species in solution. In strong support for this additional role of the DNA binding domain in self-oligomerization, LiaR<sup>(DBD)D191N</sup> formed dimers much more strongly than wild-type LiaR with a dissociation constant of the  $K_d$  to be  $< 0.04 \mu\text{M}$  (Figure 4). The association of LiaR<sup>(DBD)D191N</sup> to a dimer was so strong we could only estimate the  $K_d$  to be  $< 0.04 \mu\text{M}$ , effectively making the DNA binding domain nearly entirely dimeric under these solution conditions. Additionally, gel filtration chromatography of the isolated



**B**

Protein(s)	Best Fit Model	$K_d$ [ $\mu$ M]	95% confidence limits [ $\mu$ M]
LiaR	dimer - tetramer	24	$3.2 < K_d < 127$
LiaR <sup>D50E</sup>	dimer - tetramer	2	$0.14 < K_d < 6.0$
LiaR <sup>D191N</sup>	dimer - tetramer	0.06	$K_d < 0.06$
LiaR <sup>(DBD)</sup>	monomer - dimer	2	$0.7 < K_d < 3.4$
LiaR <sup>(DBD)D191N</sup>	monomer - dimer	0.04	$K_d < 0.04$

**Figure 4.** The adaptive mutation D191N mutation in LiaR promotes higher order complex formation. Sedimentation equilibrium analytical ultracentrifugation analysis for (A) LiaR (cyan), LiaR<sup>D50E</sup> (light green) or LiaR<sup>D191N</sup> (blue), and (B) LiaR<sup>(DBD)</sup> (dark green), LiaR<sup>(DBD)D191N</sup> (magenta). For simplicity, a representative dataset recorded at 14 000 rpm for LiaR, LiaR<sup>D50E</sup> and LiaR<sup>D191N</sup> or 36 000 rpm for LiaR<sup>(DBD)</sup> and LiaR<sup>(DBD)D191N</sup> are shown. Sedimentation equilibrium profiles for each protein were fitted to either a dimer $\leftrightarrow$ tetramer (A) or a monomer $\leftrightarrow$ dimer (B) self-association model, depicted by the black lines. The residuals for each fit are provided in the lower panel, below the experimental data.

DBD shows that DBD of LiaR<sup>D191N</sup> elutes at times consistent for a monomer to dimer transition (data not shown). The trend of increasing dimerization by LiaR<sup>(DBD)D191N</sup> parallels the trend to increased DNA binding that results from this mutation. Formation of a dimer comprised of the helix-turn-helix motifs in the LiaR DNA binding domain would be consistent with the strong and specific DNA binding we observed in our MST studies with both full-length LiaR and its isolated DNA binding domain. Our observation that LiaR<sup>(DBD)D191N</sup> has only a 50-fold higher propen-

sity for oligomerization compared to the 400-fold increase in tetramer formation seen for LiaR<sup>D191N</sup> leads us to speculate that the mutation D191N in the DNA binding domain of LiaR may change the dynamics of the entire LiaR molecule such that a change in the DNA binding domain may propagate into the receiver domain to promote further dimerization contacts.

### Structures of the LiaR<sup>(DBD)D191N</sup> with consensus and secondary DNA target sequences

To understand the atomic basis for specific DNA recognition by LiaR, we determined the structures of the DNA binding domains of wild-type LiaR (LiaR<sup>(DBD)</sup>), and LiaR<sup>D191N</sup> (LiaR<sup>(DBD)D191N</sup>) proteins alone as well as LiaR<sup>(DBD)D191N</sup> bound to DNA sequences derived from the *liaXYZ* consensus and secondary sequences by X-ray crystallography (Supplementary Table S1). The structures of LiaR<sup>(DBD)</sup> and LiaR<sup>(DBD)D191N</sup> are essentially the same with overall root mean square deviations (rmsd) of 0.4 Å (37). The domain architecture and quaternary arrangement is consistent with previously reported NarL/FixJ family DNA binding domain dimers, such as VraR, NarL, DosR and GerE in the activated state (38–41). As shown in Figure 5A and Supplementary Figure S1 the C-terminal DNA binding domain of LiaR is comprised of four  $\alpha$ -helices where the two central helices  $\alpha$ -3 from each promoter form a classic helix-turn-helix DNA binding motif. The dimer interface consists primarily of van der Waals contacts between helix-4 of protomer 1 and helix-4 of protomer 2 as well as several potential hydrogen bonds between interfacial residues. The orientation of helix-4 often varies among response regulators and is typically the product of specific but poorly conserved non-polar interactions across the dimer interface. Within the NarL/FixJ family the orientation of helix-4 from each protomer ranges from being almost parallel to one another in the case of NarL and VraR to projecting away from one another such that the two C-termini is spaced more widely than the two N-termini to make an almost V-shaped arrangement for GerE (38,39). In the LiaR–DNA structures, the dimerization helices are oriented almost parallel to each other, a case more similar to NarL and DosR than to GerE. Interestingly, both LiaR<sup>(DBD)</sup> and LiaR<sup>(DBD)D191N</sup> crystallize as dimers. This is consistent with our AUC studies suggesting a predominately dimeric quaternary structure. While position 191 is located near the dimer interface, a comparison of the main and side chain positions of Asp-191 from the LiaR<sup>(DBD)</sup> and Asn-191 of LiaR<sup>(DBD)D191N</sup> (Figure 6A) showed no significant changes in stereochemistry or potentially altered interactions through the  $\delta$ -NH<sub>2</sub> of Asn-191. The absence of significant structural changes is consistent with a more indirect effect on dimerization perhaps by stabilizing the folded state or the state that is most competent to forming the dimer. As shown in Figure 6B, there is a change in the electrostatic surface of the DNA binding surface due to the change from a negatively charged carboxylic acid group to a polar but uncharged carboxamide sidechain. We speculate that this electrostatic change (an overall less negatively charged surface) could explain both the observed increased DBD dimerization and tighter DNA binding.

In addition to structures of the LiaR<sup>(DBD)</sup> and LiaR<sup>(DBD)D191N</sup>, we determined the structure of LiaR<sup>(DBD)D191N</sup> bound to DNA sequences derived from the *liaXYZ* consensus and secondary sites (Figure 5B, C). The structure of the uncomplexed LiaR<sup>(DBD)D191N</sup> dimer is also similar to that of DNA complexes with an rmsd of 0.6 and 0.9 Å for the consensus and secondary sequence complexes. Furthermore, the buried surface areas within the dimeriza-

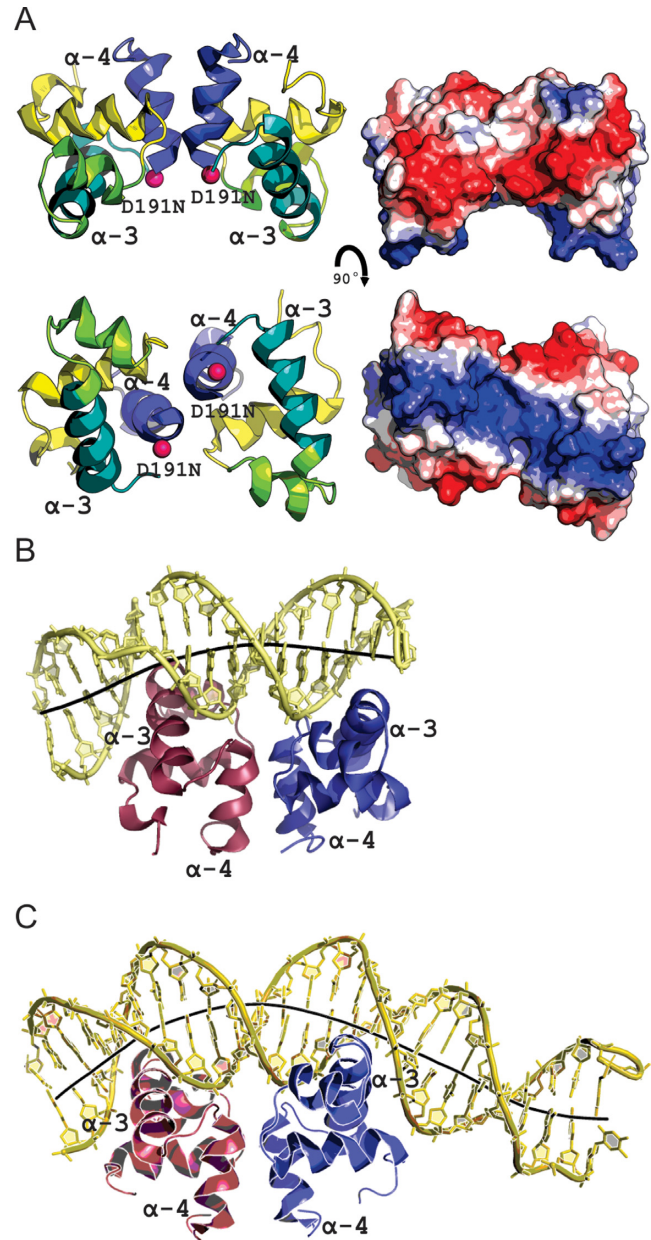


**Figure 5.** The structure of LiaR<sup>(DBD)D191N</sup> bound to DNA sequences derived from the *liaXYZ* consensus and secondary sequences. (A) Structural overview of the isolated DNA binding domain of LiaR<sup>D191N</sup>. The  $\alpha$ 4 helices of the LiaR<sup>(DBD)</sup> (blue) forms part of the molecular recognition surface responsible for formation of the functional dimer required for DNA binding. DNA-recognition helices ( $\alpha$ 3 from each promoter) are indicated in green. The two  $\alpha$ 3 helices in the dimer are positioned to create a large electropositive DNA-binding surface. (B, C) LiaR<sup>(DBD)D191N</sup> bound to DNA sequences derived from the *liaXYZ* consensus and secondary sites. The LiaR–DNA complex structure shows a strong bend in the DNA, as shown by its helical axis (gray). The helical axis calculated by the program CURVES+ (48) indicated an overall bend of 23.8° and 51.4° for the consensus (B) and secondary (C) sequences, respectively.

tion interface for the two LiaR<sup>(DBD)D191N</sup>:DNA complexes are comparable to the uncomplexed LiaR<sup>(DBD)D191N</sup> dimer (~440Å) suggesting that there are no large conformational changes within the LiaR<sup>DBD</sup> dimer upon DNA binding. The arrangement of the two helix-turn-helix motifs in the

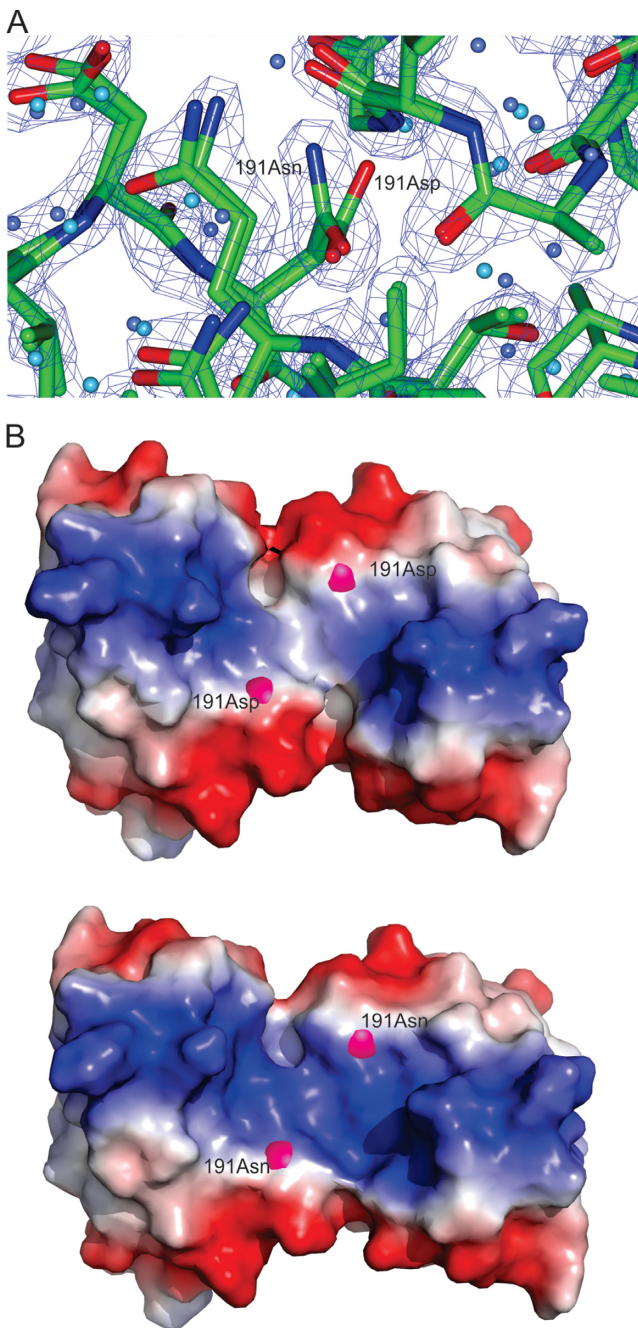


**Figure 6.** LiaR<sup>(DBD)D191N</sup> and LiaR<sup>DBD</sup> homodimer shown as both a cartoon and electrostatic surface representation. (A) Close up comparison of the main and side chain positions of Asp-191 from the LiaR<sup>(DBD)</sup> and Asn-191 of LiaR<sup>(DBD)D191N</sup> showed no significant changes in stereochemistry or potentially altered interactions. The (2FOFCWT-PH2FOFCWT) electron density map around Asn191 is contoured at 0.9 absolute value of electrons/Å<sup>3</sup>. (B) The electrostatic surface (charge surface) of the DNA binding domain of LiaR and LiaR<sup>D191N</sup> has been calculated. The magenta spheres highlight the position of amino acid 191. Red is negatively charged and blue is positive and there is a color gradient between the two (white being neutral). The DNA binding surface does become slightly more positively charged due to the D191N mutation and therefore more favorable for DNA binding.

dimer creates a positively charged surface and positioning the two helices ( $\alpha$ -3 from each promoter) at the appropriate spacing and relative orientation required for insertion into the major groove of DNA (Figure 5A), which has been observed previously for the DosR and NarL DNA complexes (38,40,41). DNA recognition by LiaR is comprised largely of residues from helix-3 (Figures 7A, B and 8). As might be expected from the DNA binding studies that showed the highest affinity for the *liaXYZ* consensus sequence, there are more base specific contacts to the DNA in the LiaR<sup>(DBD)D191N</sup>:*liaXYZ* consensus sequence complex than the LiaR<sup>(DBD)D191N</sup>:*liaXYZ* secondary sequence complex (Figure 8). In the LiaR<sup>(DBD)D191N</sup>:*liaXYZ* consensus sequence complex, Lys-174(A/B), Lys-177(A/B), Thr-178(B) are all in position to make specific H-bonds to bases of the consensus sequence (Figures 7A and 8, Supplementary Figure S2) while in the complex to the secondary sequence, only Lys-174(A/B) and Thr-178(A) have the potential make direct H-bonds (Figures 7B and 8, Supplementary Figure S2). While the consensus and secondary sequences have no discernable sequence homology, the molecular recognition surface and many of the comparable residues from LiaR that contact the DNA are largely the same.

Based on a structure-based sequence alignment of LiaR with the related response regulators DosR and NarL, LiaR Lys-177 is equivalent to Lys-188 of NarL and Lys-182 of DosR (40). In all three response regulators, different DNA sequences are accommodated by a flexible interaction to the major groove either directly or via bridging waters (40). Interestingly, Lys-177 of both chains (A, B) is involved in recognition of the *liaXYZ* consensus sequence, while there are essentially no contacts between Lys-177 and the DNA of the secondary site. Thus Lys-177 and the homologous residues in DosR and NarL appear to be important for consensus sequence recognition. Within the context of the T(X)<sub>4</sub>C(X)<sub>4</sub>G(X)<sub>4</sub>A *liaXYZ* consensus sequence, LiaR makes base specific contacts from the Ne of Lys-177(B) to the O6 of G(-94) opposite the consensus sequence C(-94) (boxed) and from the Ne of Lys-177(A) to the O6 of G(-89) (boxed). Thus in both copies of the LiaR dimer, Lys177 makes the same interaction to guanines of the consensus sequence. Similarly, Lys-174(A) and (B) are poised to make H-bonds to the O6 positions of G(-86) and G(-97) respectively, though these are not conserved consensus sequence nucleotides. Thr-178(B) of helix-3 makes non-bonded close contacts (<3.5 Å) with C(-98) of the consensus sequence. In the LiaR<sup>(DBD)D191N</sup>:*liaXYZ* secondary sequence complex, Thr-178(B) also makes a non-bonded close contact with G(-120). LiaR Thr-178 is equivalent to Val-189 of NarL and Asn-183 of DosR, and in both structures the equivalent residue makes comparable close contacts to the DNA. Significant bending of the DNA is also observed for both LiaR:DNA complexes (40) and is consistent with our DFACE studies suggesting significant structural changes to the DNA upon LiaR binding (Figures 2 and 5B, C).

#### DNA sequences near the *liaXYZ* operon may be predisposed to bending

DNase I mapping of the *liaXYZ* -320 to +30 region in the absence of protein showed a strong hypersensitive position

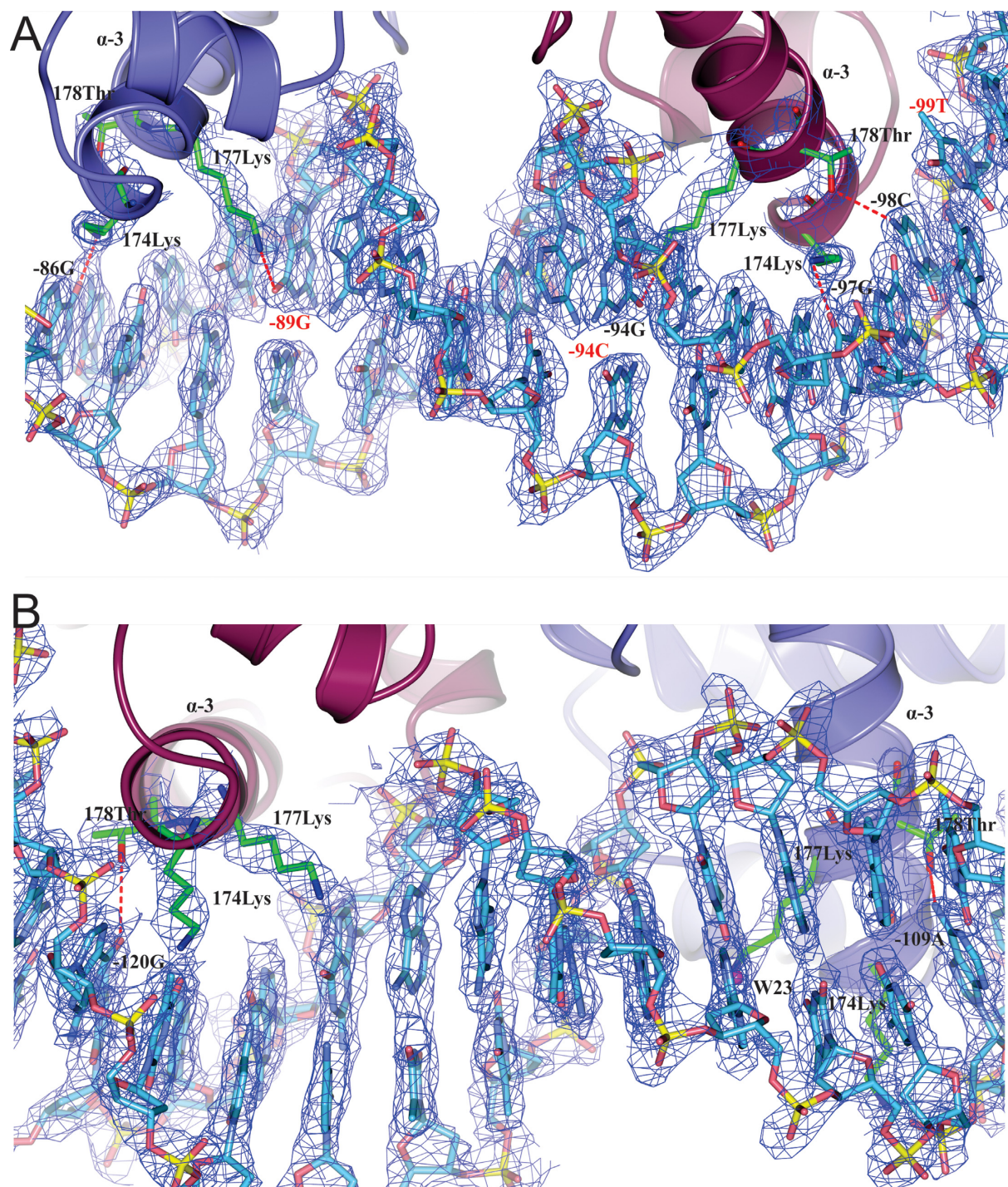


**Figure 7.** Expanded view of the binding interface of the of LiaR<sup>(ΔDBD)D191N</sup> bound to DNA sequences derived from the *liaXYZ* consensus and secondary sites. (A, B) The FEMs (Feature Enhanced Maps) are modified  $2mF_{\text{obs}} - DF_{\text{model}}$   $\sigma_A$ -weighted maps computed using phenix to reduce the model bias and retain the existing features (26). The (FEM-PHIFEM) electron density map is contoured at 0.6 absolute value of electrons/Å<sup>3</sup> to show how Lys174, Lys177 and Thr178 interact with DNA. The consensus sequence bases are indicated as red color.

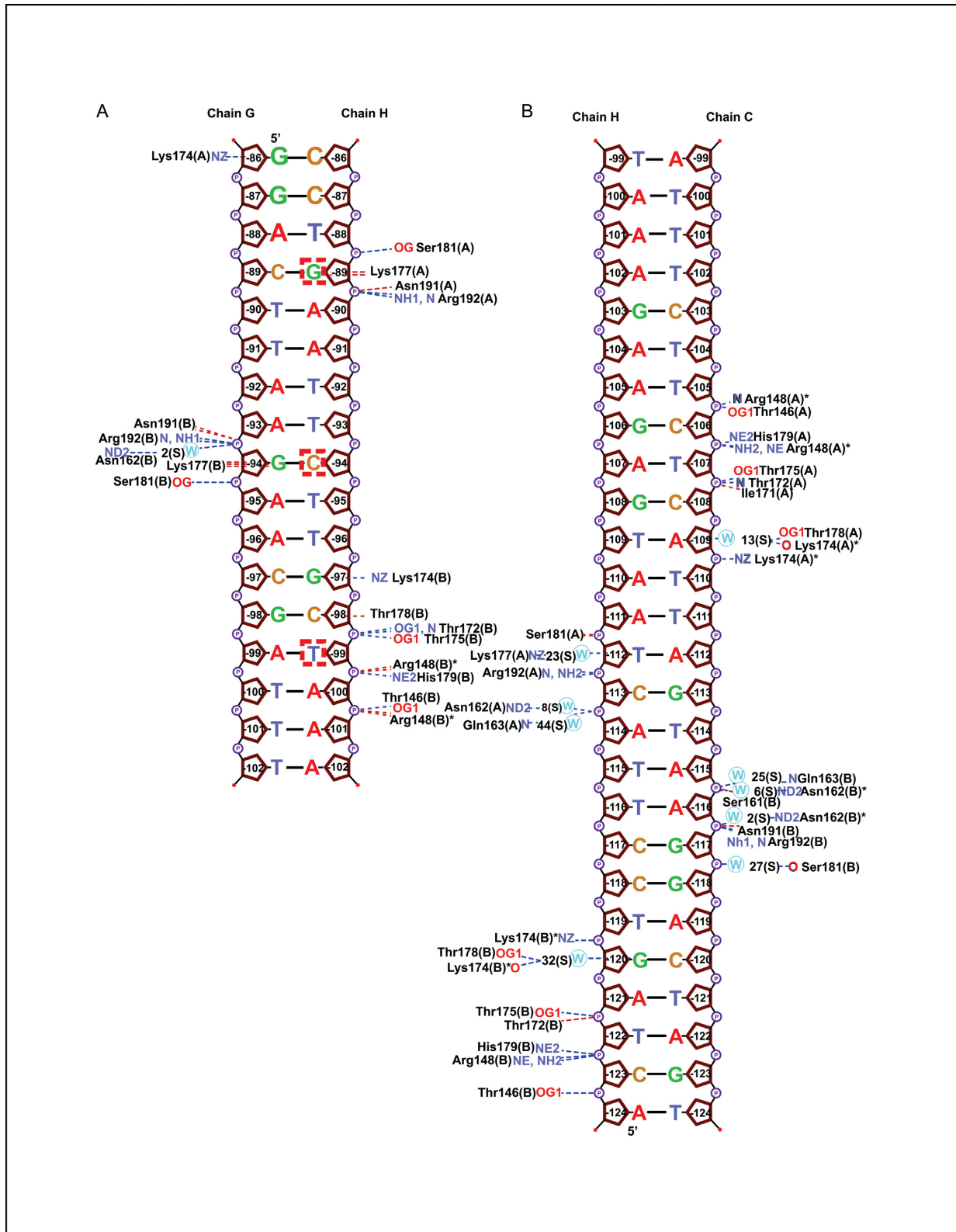


**Figure 8.** Schematic diagram of LiaR<sup>(ΔDBD)D191N</sup> bound to DNA sequences derived from the *liaXYZ* consensus and secondary sites. Base numbers are relative to the LiaX translation start site. LiaR–DNA interactions and atoms are indicated as: hydrogen bonds (blue dotted lines); non-bonded contacts (red dotted lines); nitrogens (blue lettering); oxygens (red lettering); and waters (blue circles). The conserved consensus sequence nucleotides which we identified using *in silico* analysis G, C and T are boxed (T(X)<sub>4</sub>C(X)<sub>4</sub>G(X)<sub>4</sub>A).

at T(-35) consistent with increased nuclease accessibility. Upon addition of LiaR to 0.5  $\mu\text{M}$  the hypersensitive location shifts to C(-36), and at 5.0  $\mu\text{M}$  protein the hypersensitive site shifts further to C(-38) suggesting that LiaR binding at -120 to -77 has a strong effect on the 3' distal DNA structure (Figure 2E). While it is possible that the original hypersensitive site is the product of a unique DNA sequence context, it was striking that the position of the hypersensitive site shifts upon formation of the LiaR-DNA complex and that the position is within the putative footprint region of RNAP polymerase binding to canonical -10/-35 regions of DNA during the initiation of transcription. Taken together with proximal hypersensitive sites found for both the *liaFSR* and *liaXYZ* at the nucleotide following the adenine in the T(X)<sub>4</sub>C(X)<sub>4</sub>G(X)<sub>4</sub>A consensus sequences and the crystal structures of LiaR DNA binding domains bound to target DNA, it is apparent that LiaR binding imposes changes to DNA structure consistent with DNA bending.

#### A model for binding to extended DNA regulatory sequences by an activated LiaR tetramer

As shown in Figure 9, a LiaR tetramer would have four helix-turn-helix motifs potentially able to span  $\sim 42$  nucleotides. The observed protection site for the *liaXYZ* operon was 44 nucleotides. The protection site for the *liaFSR* operon appears smaller and is more consistent with three of the four potential DNA binding domains making strong interactions with the DNA. Our data suggests that the LiaR tetramer can be thought of as having four DNA reading heads that can each recognize and bind DNA depending on the organization of the upstream regulatory DNA sequences. In the *liaXYZ* operon, all four DNA reading heads are tightly associated with the DNA while in the case of the *liaFSR* operon three of the four reading heads are making strong contacts to the DNA leading to protection. Presumably since the fourth reading head is present, its interaction with DNA is too weak to produce detectable levels of DNA protection. Based upon the combination of these results we have constructed a model for how LiaR might bind to an extended DNA sequences through the two sets of helix-turn helix dimers that would be present in the LiaR tetramer (Figure 9). The orientation of the DNA binding domains from the crystallographic LiaR-DNA co-structures and increase in DNA hypersensitivity observed by our DFACE studies (Figure 2) suggest that the binding of LiaR will induce DNA bending. We speculate that increased DNA bending could recruit RNA polymerase through direct protein contacts and may favor formation of the pre-initiation bubble. Transcription factors (42) are divided into two classes based on their interactions with the RNA polymerase holoenzyme. Class I factors, such as BvgA (15) and OmpR (43) interact with the C-terminal domain of the subunit  $\alpha$ -of RNAP while Class II factors, such as PhoB (44) and VanR (45) interact with the RNA polymerase sigma-subunit. The closest homolog of LiaR, VraR from *S. aureus* has been shown to interact with the sigma-subunit of RNA polymerase (29).

To construct a potential model for LiaR-mediated regulation, we joined the DNA sequences of the *E. coli* RNA polymerase initiation complex (3IYD) with those of our

LiaR<sup>D191N</sup> DNA binding domains complexed with the sequences derived from the *liaXYZ* consensus and secondary sites (dark red, PDB: 4WUL and 4WU4) modeled as an active tetramer using the protein alone available tetramer structure of the *S. aureus* VraR receiver domains (pink; PDB: 4IF4) (46). The resulting combined model is striking in its clear positioning of LiaR through DNA bending to make potential contacts with RNA polymerase. DNA bending has been observed frequently for other transcription factors and is consistent with enhanced recruitment of RNA polymerase to increase transcription. As shown in Figure 9, the LiaR tetramer is potentially well poised to recruit and interact with RNA polymerase at the promoter.

#### CONCLUSION

The cell envelope stress response of Gram-positive organisms is intimately associated with their ability to adapt to membrane damaging antibiotics such as daptomycin and other antimicrobial peptides. Mutations within the LiaFSR signaling pathway are often observed as part of the development of antibiotic resistance in the pathogens that are designated as high priorities for control by the CDC such as enterococci and *S. aureus*. Adaptive mutations such as LiaR<sup>D191N</sup> that lead to daptomycin resistance can activate the *liaFSR* regulon in a phosphorylation independent manner, by inducing the formation of the oligomeric states responsible for sequence specific DNA recognition (Figure 1). It is clear from our work, as well as that of others, that while there are some key similarities in the general principles describing LiaFSR and LiaFSR-like homologs for the regulation of target operons, there are important distinctions that can be used to enhance our understanding of these important systems. Strategies that would develop small molecules to inhibit the development of resistance should be cognizant of the differences between these systems in order to have the broadest efficacy.

In *B. subtilis*, *E. faecalis*, *L. monocytogenes* LiaR and *S. aureus* VraR there is clear evidence for consensus binding sites though there are significant variations within and among the organisms suggesting that a more complex and subtle DNA recognition strategy is common (6,30,47). Despite the fact that members of the NarL/FixJ response regulator family like *E. faecalis* LiaR and *S. aureus* VraR share a conserved domain structure and sequence specific DNA recognition via well conserved helix-turn-helix motifs and high overall sequence similarity, there are no obvious similarities to their DNA-binding consensus sequence (30). Presumably subtle changes in the interaction of the helix-turn-helix motifs with DNA targets are responsible for the wide range of recognition sequences across related response regulators. Even within the two operons we studied from *E. faecalis* S613 there are important differences in position and composition of the DNA regulatory elements. Our DNA binding studies indicate that for the *liaXYZ* operon, tight binding is achieved readily by the consensus sequence and that the extended secondary sequence, though protected in footprinting, does not contribute significantly to overall DNA affinity by LiaR (Table 1). In contrast, binding to the *liaFSR* operon consensus sequence is weak and that only upon including regions outside the canonical consensus se-

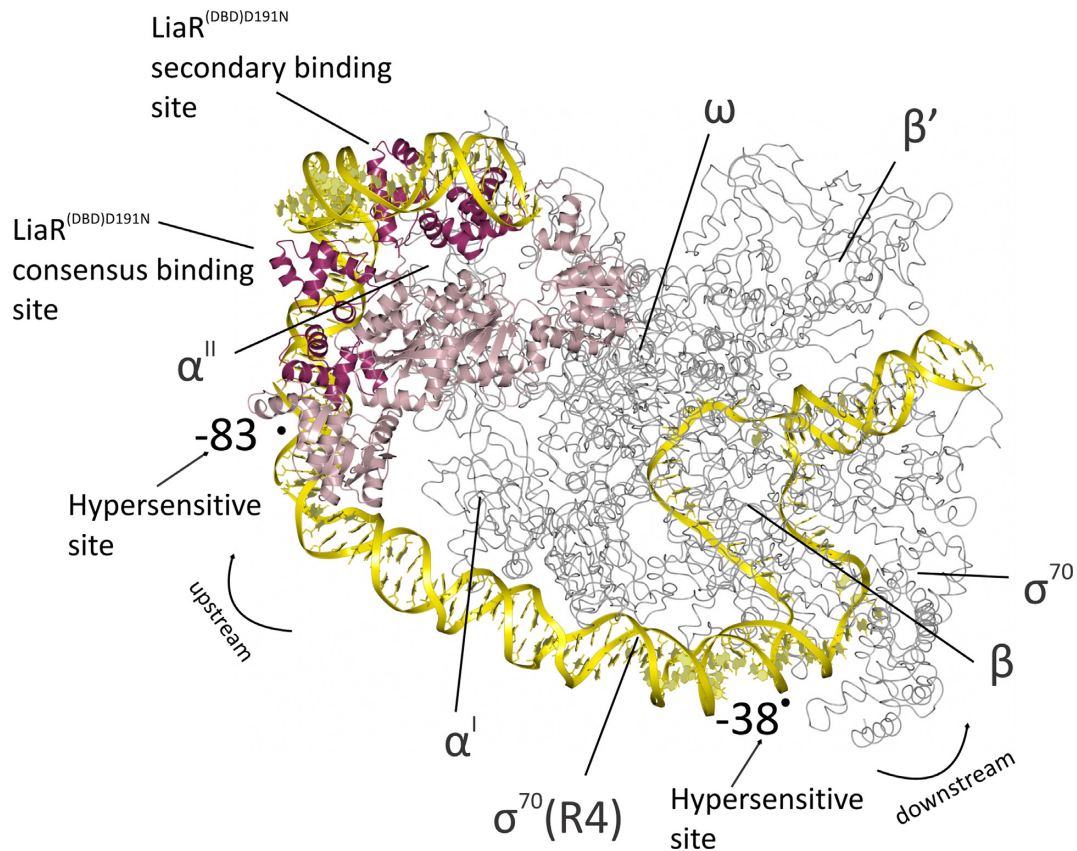


**Figure 9.** Model for the binding of the activated LiaR tetramer onto the regulatory sequences responsible for the LiaR-mediated cell envelope stress response. The LiaR<sup>D191N</sup> DNA binding domains bound to DNA sequences derived from the *liaXYZ* consensus and secondary sites (dark red; PDB: 4WUL and 4WU4) are modeled as an active tetramer using the protein alone tetramer structure of the *S. aureus* VraR receiver domains (pink; PDB: 4IF4). The structure of the *E. coli* RNA polymerase complex initiation complex (gray; PDB: 3IYD) was used to model the position of RNA polymerase and DNA. The combined model for the LiaR:DNA and RNA polymerase:DNA complexes (yellow) suggests a strong bend that is consistent with the crystal structures and DNaseI hypersensitive sites from our protection studies (arrows). Note that the RNA polymerase  $\alpha'$  and  $\omega$  subunits are well poised for potential interactions with the LiaR tetramer.

quence is high affinity achieved. Our DNA footprinting and analytical ultracentrifugation studies indicate an extended DNA recognition site consistent with the formation of an activated tetramer.

Interestingly, although solution studies indicate a phosphorylation-dependent monomer–dimer equilibrium for VraR, the activated protein crystallized as a tetramer, suggesting that there may be a role for higher-order oligomers. DNA footprinting studies show that, like *E. faecalis* LiaR, VraR has a larger than expected recognition site upstream of *vraSR*, upon phosphorylation, that would exceed the size protected by a single VraR dimer (30) and includes DNase I hypersensitive sites indicative of DNA bending. Activation of transcription may require significant DNA bending, involving 4 protein molecules (either as a pair of dimers or a single tetramer), necessary to recruit RNA polymerase (Figure 9) (30) to form the transcription initiation complex. The quaternary structure of LiaR and related cell envelope stress response pathways such as *S. aureus* VraR may share a common evolutionary monomer–dimer–tetramer equilibrium and that, over time, organisms have adapted both in the sequence of the DNA regulatory elements as well as the LiaR quaternary

structure equilibrium to provide a well-adapted stress response. In principle, the equilibrium constants for a response regulator monomer–dimer and dimer–tetramer can be tuned readily to provide the appropriate level of response. *E. faecium* LiaR shares 84% identity with that of *E. faecalis* S613 and 60% with *S. aureus* VraR and therefore its solution binding properties and organization of the target operon regulatory elements could resemble either homolog and will have to await further study. So while there are some similarities between LiaR homologs of *B. subtilis* and *S. aureus*, the sequences recognized and the manner in which they are recognized and presumably regulated has changed to fit the specific ecological and evolutionary challenges that confront these organisms. Presumably the membrane stress response pathways of these organisms reflect that distinct evolutionary history.

#### ACCESSION NUMBERS

wwPDB: 4WSZ, 4WT0, 4WUH, 4WU4, 4WUL.

#### SUPPLEMENTARY DATA

Supplementary Data are available at NAR Online.

## ACKNOWLEDGEMENTS

We thank the staff at ANL APS for their training and support during the data collection.

*Authors contributions:* M.D., C.A.A. and Y. S. designed research, analysed data, and wrote the paper; M.D., Y.S., T.A.J., P.G.L., and M.Z. performed the experiments. P.G.L., J.E.L. edited the manuscript.

## FUNDING

National Institutes of Health Grant [R01AI080714 to Y.S.]; The Rice University Crystallographic Core Facility is supported by a Kresge Science Initiative endowment grant. Funding for open access charge: National Institutes of Health Grant [R01AI080714 to Y.S.].

*Conflict of interest statement.* Cesar A. Arias has received grant support, consulted for or provided lectures for Pfizer, Cubist, Bayer, Forest Pharmaceuticals, Novartis, and Theravance.

## REFERENCES

- Boucher, H.W., Talbot, G.H., Bradley, J.S., Edwards, J.E., Gilbert, D., Rice, L.B., Scheld, M., Spellberg, B. and Bartlett, J. (2009) Bad bugs, no drugs: no ESKAPE! an update from the Infectious Diseases Society of America. *Clin. Infect. Dis.*, **48**, 1–12.
- Rice, L.B. (2008) Federal funding for the study of antimicrobial resistance in nosocomial pathogens: no ESKAPE. *J. Infect. Dis.*, **197**, 1079–1081.
- Arias, C.A. and Murray, B.E. (2012) The rise of the Enterococcus: beyond vancomycin resistance. *Nat. Rev. Microbiol.*, **10**, 266–278.
- Arias, C.A., Panesso, D., McGrath, D.M., Qin, X., Mojica, M.F., Miller, C., Diaz, L., Tran, T.T., Rincon, S., Barbu, E.M. *et al.* (2011) Genetic basis for in vivo daptomycin resistance in enterococci. *N. Engl. J. Med.*, **365**, 892–900.
- Miller, C., Kong, J., Tran, T.T., Arias, C.A., Saxer, G. and Shamooy, Y. (2013) Adaptation of Enterococcus faecalis to daptomycin reveals an ordered progression to resistance. *Antimicrob. Agents Chemother.*, **57**, 5373–5383.
- Wolf, D., Kalamorz, F., Wecke, T., Juszczak, A., Mader, U., Homuth, G., Jordan, S., Kirstein, J., Hoppert, M., Voigt, B. *et al.* (2010) In-depth profiling of the LiaR response of Bacillus subtilis. *J. Bacteriol.*, **192**, 4680–4693.
- Jordan, S., Junker, A., Helmann, J.D. and Mascher, T. (2006) Regulation of LiaRS-dependent gene expression in bacillus subtilis: identification of inhibitor proteins, regulator binding sites, and target genes of a conserved cell envelope stress-sensing two-component system. *J. Bacteriol.*, **188**, 5153–5166.
- McCallum, N., Meier, P.S., Heusser, R. and Berger-Bachi, B. (2011) Mutational analyses of open reading frames within the vraSR operon and their roles in the cell wall stress response of Staphylococcus aureus. *Antimicrob. Agents Chemother.*, **55**, 1391–1402.
- Schrecke, K., Jordan, S. and Mascher, T. (2013) Stoichiometry and perturbation studies of the LiaFSR system of Bacillus subtilis. *Mol. Microbiol.*, **87**, 769–788.
- Munita, J.M., Panesso, D., Diaz, L., Tran, T.T., Reyes, J., Wanger, A., Murray, B.E. and Arias, C.A. (2012) Correlation between mutations in liaFSR of Enterococcus faecalis and MIC of daptomycin: revisiting daptomycin breakpoints. *Antimicrob. Agents Chemother.*, **56**, 4354–4359.
- Munita, J.M., Tran, T.T., Diaz, L., Panesso, D., Reyes, J., Murray, B.E. and Arias, C.A. (2013) A liaF codon deletion abolishes daptomycin bactericidal activity against vancomycin-resistant Enterococcus faecalis. *Antimicrob. Agents Chemother.*, **57**, 2831–2833.
- Palmer, K.L., Daniel, A., Hardy, C., Silverman, J. and Gilmore, M.S. (2011) Genetic basis for daptomycin resistance in enterococci. *Antimicrob. Agents Chemother.*, **55**, 3345–3356.
- Reyes, J., Panesso, D., Tran, T.T., Mishra, N.N., Cruz, M.R., Munita, J.M., Singh, K.V., Yeaman, M.R., Murray, B.E., Shamooy, Y. *et al.* (2014) A liaR deletion restores susceptibility to daptomycin and antimicrobial peptides in multidrug-resistant Enterococcus faecalis. *J. Infect. Dis.*, **211**, 1317–1325.
- Park, D.M., Akhtar, M.S., Ansari, A.Z., Landick, R. and Kiley, P.J. (2013) The bacterial response regulator ArcA uses a diverse binding site architecture to regulate carbon oxidation globally. *PLoS Genet.*, **9**, e1003839.
- Boucher, P.E., Maris, A.E., Yang, M.S. and Stibitz, S. (2003) The response regulator BvgA and RNA polymerase alpha subunit C-terminal domain bind simultaneously to different faces of the same segment of promoter DNA. *Mol. Cell.*, **11**, 163–173.
- Griffith, K.L. and Grossman, A.D. (2008) A degenerate tripartite DNA-binding site required for activation of ComA-dependent quorum response gene expression in Bacillus subtilis. *J. Mol. Biol.*, **381**, 261–275.
- Olekhovich, I.N. and Kadner, R.J. (1999) RNA polymerase alpha and sigma(70) subunits participate in transcription of the Escherichia coli uhpT promoter. *J. Bacteriol.*, **181**, 7266–7273.
- Saxer, G., Krepps, M.D., Merkley, E.D., Ansong, C., Deatherage Kaiser, B.L., Valovska, M.T., Ristic, N., Yeh, P.T., Prakash, V.P., Leiser, O.P. *et al.* (2014) Mutations in global regulators lead to metabolic selection during adaptation to complex environments. *PLoS Genet.*, **10**, e1004872.
- Zianni, M., Tessanne, K., Merighi, M., Laguna, R. and Tabita, F.R. (2006) Identification of the DNA bases of a DNase I footprint by the use of dye primer sequencing on an automated capillary DNA analysis instrument. *J. Biomol. Tech.*, **17**, 103–113.
- Joshi, G.S., Zianni, M., Bobst, C.E. and Tabita, F.R. (2012) Further unraveling the regulatory twist by elucidating metabolic coinducer-mediated CbbR-cbbI promoter interactions in Rhodospseudomonas palustris CGA010. *J. Bacteriol.*, **194**, 1350–1360.
- Jerabek-Willemsen, M., Wienken, C.J., Braun, D., Baaske, P. and Duhr, S. (2011) Molecular interaction studies using microscale thermophoresis. *Assay Drug Dev. Technol.*, **9**, 342–353.
- Vistica, J., Dam, J., Balbo, A., Yikilmaz, E., Mariuzza, R.A., Rouault, T.A. and Schuck, P. (2004) Sedimentation equilibrium analysis of protein interactions with global implicit mass conservation constraints and systematic noise decomposition. *Anal. Biochem.*, **326**, 234–256.
- Schuck, P. (2003) On the analysis of protein self-association by sedimentation velocity analytical ultracentrifugation. *Anal. Biochem.*, **320**, 104–124.
- McCoy, A.J., Grosse-Kunstleve, R.W., Adams, P.D., Winn, M.D., Storoni, L.C. and Read, R.J. (2007) Phaser crystallographic software. *J. Appl. Crystallogr.*, **40**, 658–674.
- Kantardjiev, K.A. and Rupp, B. (2003) Matthews coefficient probabilities: Improved estimates for unit cell contents of proteins, DNA, and protein-nucleic acid complex crystals. *Protein Sci.*, **12**, 1865–1871.
- Adams, P.D., Afonine, P.V., Bunkoczi, G., Chen, V.B., Davis, I.W., Echols, N., Headd, J.J., Hung, L.W., Kapral, G.J., Grosse-Kunstleve, R.W. *et al.* (2010) PHENIX: a comprehensive Python-based system for macromolecular structure solution. *Acta Crystallogr. D Biol. Crystallogr.*, **66**, 213–221.
- Emsley, P. and Cowtan, K. (2004) Coot: model-building tools for molecular graphics. *Acta Crystallogr. D Biol. Crystallogr.*, **60**, 2126–2132.
- Chen, V.B., Arendall, W.B. 3rd, Headd, J.J., Keedy, D.A., Immormino, R.M., Kapral, G.J., Murray, L.W., Richardson, J.S. and Richardson, D.C. (2010) MolProbity: all-atom structure validation for macromolecular crystallography. *Acta Crystallogr. D Biol. Crystallogr.*, **66**, 12–21.
- Belcheva, A., Verma, V., Korenevsky, A., Fridman, M., Kumar, K. and Golemi-Kotra, D. (2012) Roles of DNA sequence and sigma A factor in transcription of the vraSR operon. *J. Bacteriol.*, **194**, 61–71.
- Belcheva, A., Verma, V. and Golemi-Kotra, D. (2009) DNA-binding activity of the vancomycin resistance associated regulator protein VraR and the role of phosphorylation in transcriptional regulation of the vraSR operon. *Biochemistry*, **48**, 5592–5601.
- Belcheva, A. and Golemi-Kotra, D. (2008) A close-up view of the VraSR two-component system. A mediator of Staphylococcus aureus response to cell wall damage. *J. Biol. Chem.*, **283**, 12354–12364.

32. Leonard, P.G., Golemi-Kotra, D. and Stock, A.M. (2013) Phosphorylation-dependent conformational changes and domain rearrangements in *Staphylococcus aureus* VraR activation. *Proc. Natl. Acad. Sci. U.S.A.*, **110**, 8525–8530.
33. Steidl, R., Pearson, S., Stephenson, R.E., Ledala, N., Sitthisak, S., Wilkinson, B.J. and Jayaswal, R.K. (2008) *Staphylococcus aureus* cell wall stress stimulon gene-lacZ fusion strains: potential for use in screening for cell wall-active antimicrobials. *Antimicrob. Agents Chemother.*, **52**, 2923–2925.
34. Stock, A.M., Robinson, V.L. and Goudreau, P.N. (2000) Two-component signal transduction. *Annu. Rev. Biochem.*, **69**, 183–215.
35. Cai, S.J. and Inouye, M. (2002) EnvZ-OmpR interaction and osmoregulation in *Escherichia coli*. *J. Biol. Chem.*, **277**, 24155–24161.
36. Gegner, J.A., Graham, D.R., Roth, A.F. and Dahlquist, F.W. (1992) Assembly of an MCP receptor, CheW, and kinase CheA complex in the bacterial chemotaxis signal transduction pathway. *Cell*, **70**, 975–982.
37. Krissinel, E. and Henrick, K. (2004) Secondary-structure matching (SSM), a new tool for fast protein structure alignment in three dimensions. *Acta Crystallogr. D Biol. Crystallogr.*, **60**, 2256–2268.
38. Maris, A.E., Kaczor-Grzeskowiak, M., Ma, Z., Kopka, M.L., Gunsalus, R.P. and Dickerson, R.E. (2005) Primary and secondary modes of DNA recognition by the NarL two-component response regulator. *Biochemistry*, **44**, 14538–14552.
39. Ducros, V.M., Lewis, R.J., Verma, C.S., Dodson, E.J., Leonard, G., Turkenburg, J.P., Murshudov, G.N., Wilkinson, A.J. and Brannigan, J.A. (2001) Crystal structure of GerE, the ultimate transcriptional regulator of spore formation in *Bacillus subtilis*. *J. Mol. Biol.*, **306**, 759–771.
40. Wisedchaisri, G., Wu, M., Rice, A.E., Roberts, D.M., Sherman, D.R. and Hol, W.G. (2005) Structures of *Mycobacterium tuberculosis* DosR and DosR-DNA complex involved in gene activation during adaptation to hypoxic latency. *J. Mol. Biol.*, **354**, 630–641.
41. Maris, A.E., Sawaya, M.R., Kaczor-Grzeskowiak, M., Jarvis, M.R., Bearson, S.M., Kopka, M.L., Schroder, I., Gunsalus, R.P. and Dickerson, R.E. (2002) Dimerization allows DNA target site recognition by the NarL response regulator. *Nat. Struct. Biol.*, **9**, 771–778.
42. Ishihama, A. (1993) Protein-protein communication within the transcription apparatus. *J. Bacteriol.*, **175**, 2483–2489.
43. Okamura, H., Hanaoka, S., Nagadoi, A., Makino, K. and Nishimura, Y. (2000) Structural comparison of the PhoB and OmpR DNA-binding/transactivation domains and the arrangement of PhoB molecules on the phosphate box. *J. Mol. Biol.*, **295**, 1225–1236.
44. Makino, K., Shinagawa, H., Amemura, M., Kimura, S., Nakata, A. and Ishihama, A. (1988) Regulation of the phosphate regulon of *Escherichia coli*. Activation of *pstS* transcription by PhoB protein in vitro. *J. Mol. Biol.*, **203**, 85–95.
45. Depardieu, F., Courvalin, P. and Kolb, A. (2005) Binding sites of VanRB and sigma70 RNA polymerase in the *vanB* vancomycin resistance operon of *Enterococcus faecium* BM4524. *Mol. Microbiol.*, **57**, 550–564.
46. Hudson, B.P., Quispe, J., Lara-Gonzalez, S., Kim, Y., Berman, H.M., Arnold, E., Ebright, R.H. and Lawson, C.L. (2009) Three-dimensional EM structure of an intact activator-dependent transcription initiation complex. *Proc. Natl. Acad. Sci. U.S.A.*, **106**, 19830–19835.
47. Fritsch, F., Mauder, N., Williams, T., Weiser, J., Oberle, M. and Beier, D. (2011) The cell envelope stress response mediated by the LiaFSRLm three-component system of *Listeria monocytogenes* is controlled via the phosphatase activity of the bifunctional histidine kinase LiaSLm. *Microbiology*, **157**, 373–386.
48. Blanchet, C., Pasi, M., Zakrzewska, K. and Lavery, R. (2011) CURVES+ web server for analyzing and visualizing the helical, backbone and groove parameters of nucleic acid structures. *Nucleic Acids Res.*, **39**, W68–W73.